

Brain microenvironment-remodeling nanomedicine improves cerebral glucose metabolism, mitochondrial activity and synaptic function in a mouse model of Alzheimer's disease

Elliya Park^a , Chunsheng He^a, Azhar Z. Abbasi^a, Meng Tian^b, Shudi Huang^a, Liting Wang^a, John Georgiou^c, Graham L. Collingridge^{b,c} , Paul E. Fraser^d, Jeffrey T. Henderson^a, Xiao Yu Wu^{a,*} 

^a 144 College St, Leslie Dan Faculty of Pharmacy, University of Toronto, Toronto, ON, M5S 3M2, Canada

^b 135 Nassau St, TANZ Centre for Research in Neurodegenerative Diseases, University of Toronto, Toronto, ON, M5T 1M8, Canada

^c 600 University Ave, Lunenfeld-Tanenbaum Research Institute, Mount Sinai Hospital, Toronto, ON, M5G 1X5, Canada

^d 60 Leonard Ave, Tanz Centre for Research in Neurodegenerative Diseases, Department of Medical Biophysics, University of Toronto, Toronto, ON, M5T 2S8, Canada

ARTICLE INFO

Keywords:

Blood brain barrier-crossing nanomedicine
Biocompatible hybrid manganese dioxide nanoparticles
Disease-modifying treatment of Alzheimer's disease
Glucose metabolism
Glucose utilization
Mitochondrial function
Synaptic function

ABSTRACT

The development of disease-modifying therapeutics for Alzheimer's disease remains challenging due to the complex pathology and the presence of the blood-brain barrier. Previously we have described the investigation of a brain-penetrating multifunctional bioactive nanoparticle system capable of remodeling the hypoxic and inflammatory brain microenvironment and reducing beta-amyloid plaques improving cognitive function in a mouse model of Alzheimer's disease. Despite the linkage of hypoxia and inflammation to metabolic alteration, the effects of this system on modulating cerebral glucose metabolism, mitochondrial activity and synaptic function remained to be elucidated. To examine this, a transgenic mouse model of Alzheimer's disease (TgCRND8) *in vivo* were treated intravenously with beta-amyloid antibody-conjugated (Ab), blood-brain barrier-crossing terpolymer (TP) containing polymer-lipid based manganese dioxide nanoparticles (Ab-TP-MDNPs). Alterations in cerebral glucose utilization were determined by [¹⁸F]FDG-PET imaging *in vivo*, with glucose metabolism and mitochondrial activity analyzed by biomarkers and studies with primary neurons *in vitro*. Synaptic function was evaluated by both biomarkers and electrophysiologic analysis. Current study shows that intravenously administered Ab-TP-MDNPs enhanced cerebral glucose utilization, improved glucose metabolism, mitochondrial activity, and increased the levels of neprilysin, O-glycosylation. The consequence of this was enhanced glucose and ATP availability, resulting in improved long-term potentiation for promoting neuronal synaptic function. This study highlights the importance of targeting the metabolism of complex disease pathologies in addressing disease-modifying therapeutics for neurodegenerative disorders such as Alzheimer's disease.

1. Introduction

Alzheimer's disease (AD) is a neurodegenerative disorder characterized by cognitive impairment with complex etiology. This multifaceted pathology of AD poses significant obstacles to finding effective disease-modifying therapies. Additionally, constraints of the blood-brain barrier (BBB) add further challenges to efficiently delivering therapeutics to disease loci [1]. To date, amyloid β (A β) has been a prime target in the development of disease-modifying therapies for AD [2–4].

However its originating causal role in AD pathology remains controversial, in part due to the known contributions of other neuropathologic factors in AD progression [4].

Brain hypometabolism either primary or secondary to vascular hypoperfusion is a key feature of AD [5,6]. As one of the body's most active organs in terms of glucose utilization, the brain depends intimately upon supplies of glucose as its primary source of energy. Indeed in AD, glucose hypometabolism is observed well before symptomatic disease onset, suggesting a significant role for glucose impairment in the

* Corresponding author. Leslie Dan Faculty of Pharmacy, University of Toronto, Ontario, M5S 3M2, Canada.

E-mail address: sxy.wu@utoronto.ca (X.Y. Wu).

<https://doi.org/10.1016/j.biomaterials.2025.123142>

Received 16 August 2024; Received in revised form 29 December 2024; Accepted 23 January 2025

Available online 24 January 2025

0142-9612/© 2025 The Authors. Published by Elsevier Ltd. This is an open access article under the CC BY-NC license (<http://creativecommons.org/licenses/by-nc/4.0/>).

development of AD [7]. Specifically glucose utilization within the brain undergoes an ~50% reduction during the early stages of AD, correlating with a decline in cognitive function [8,9]. Therefore, therapeutic interventions have been explored to improve cerebral metabolism in AD [10], including supplementation with lactates [11]. While preclinical results showed promise [10,12], clinical data indicate that this therapeutic effect would likely be limited to the early stages of disease progression, though it remains a major target within the current clinical trial pipeline [13].

Synaptic dysfunction is also a prominent early hallmark of AD [14]. Given its noted effects on cognitive memory in AD, drugs aimed at targeting synaptic dysfunction have been explored clinically [15]. However modifiers of synaptic function are currently limited to symptomatic alleviation, suggesting that synaptic dysfunction is just one aspect of the greater neural dysfunction observed in AD [15]. The root causes could include not only direct synaptic effects mediated through toxic isoforms of A β , but also metabolic dysfunction and oxidative stress [3].

To address the above issues, this study explores the potential multimodal effects of Ab-TP-MDNPs in altering the metabolic and synaptic dysfunctions observed in AD. Ab-TP-MDNPs employ an efficient brain-penetrating drug delivery technology, leveraging a unique terpolymer (TP) system developed in our laboratory to retard reductions in neural function seen in AD. The terpolymer consists of starch grafted poly(methacrylic acid) and polysorbate 80 to facilitate endogenous apolipoprotein E addition, promoting transfer across the BBB via low density lipoprotein receptor-mediated transcytosis [16–21]. The surface of nanoparticles is decorated with anti-A β antibody to promote adherence to A β plaques and oligomers within the brain [16]. Due to their payload, Ab-TP-MDNPs subsequently react with plaque-associated reactive oxygen species (ROS) detoxifying them to generate non-toxic local O₂. This reaction addresses several key issues in AD pathology beyond hypoxia and toxic ROS. In our previous investigations we have determined the efficacy of Ab-TP-MDNPs in reducing oxidative stress and neuroinflammation, aiding local vascular normalization, thus enhancing A β clearance and ultimately improving cognitive function in an AD mouse model [22]. In the present study, we examine the potential of intravenously administered Ab-TP-MDNPs to utilize the above functions to improve glucose utilization and metabolism within the brain of a transgenic mouse model (TgCRND8 strain) of AD to enhance cerebral neuronal function. The proposed mechanism and outcomes of Ab-TP-MDNP treatment are illustrated in Fig. 1. The results demonstrate that Ab-TP-MDNP treatment enhances brain glucose utilization, resulting in improved energy metabolism to support neuronal function. This improvement in CNS function was assessed using both functionally and electrophysiologic measures, [¹⁸F]FDG (fluorodeoxyglucose)-PET (positron emission tomography), CT (computed tomography); together with previously identified biomarkers.

To the best of our knowledge this study is the first attempt to assess functional and metabolic aspects of cerebral neurons in AD following the application of a multimodal nanoparticle treatment, in order to gain a comprehensive understanding of therapeutic outcomes associated with manganese dioxide nanoparticle treatment. These findings thus provide valuable insights into further optimizing such technology further, facilitating its transition toward clinical application for the treatment of AD.

2. Materials and methods

2.1. Materials

Soluble corn starch (molecular weight [MW] = 11,000 g/mol), methacrylic acid (MAA), sodium thiosulfate (STS), potassium persulfate (KPS), polysorbate 80 (PS 80), sodium dodecyl sulfate (SDS), N-(3-(dimethylaminopropyl)-N'-ethylcarbodiimide hydrochloride (EDC), ethyl arachidate, dextrose, phosphate-buffered saline (PBS), and Triton X-100 were purchased from Sigma-Aldrich, Canada (Oakville, ON,

Canada). All chemicals were of analytical grade and used without further purification unless otherwise indicated.

2.2. Formulation and characterization of Ab-TP-MDNPs

Brain-penetrating A β -targeted nanoparticles (Ab-TP-MDNPs) were synthesized as previously described [16]. Brain permeable terpolymer, i. e., poly(methacrylic acid) (PMAA) and polysorbate 80 (PS80) grafted starch (St) (PMAA-PS 80-g-St) was synthesized to prepare polymer-lipid nanoparticles [16–20]. Anti-A β antibody 4G8s functionalized terpolymer was obtained by conjugating 4G8 (Biolegend 800703, San Diego, CA, USA) to the polymers using well-known 1-ethyl-3-(3-dimethylaminopropyl) carbodiimide (EDC) chemistry. Briefly, Ab-TP-MDNPs were prepared using a modified “one-pot” synthesis method. The formulation process begins with the synthesis of precursor MnO₂ from KMnO₄ using polyvinyl alcohol as a reducing agent and incorporating these precursor small metal particles into the polymer-lipid matrix. The final MnO₂ carrier polymer-lipid particles were self-assembled using 4G8 functionalized terpolymers and low melting point lipids under ultrasound sonication at 80% peak (Hielscher UP 100H probe ultrasonicator, Ringwood, NJ, USA). Lastly, the obtained nanoparticles solution was purified against doubly distilled deionized water (DDIW) using the Minimate™ Tangential Flow Filtration Systems (Pall Corporation, Mississauga, ON, CA) and the purified nanoparticles were lyophilized in the presence of a cryoprotectant glucose (1 w/v%) to obtain the dried powder for further use. The particle size and zeta potential of the lyophilized Ab-TP-MDNPs were measured using the Malvern Zetasizer Nano ZS (Worcestershire, UK) (data not shown). The concentration of MnO₂ in the polymer-lipid formulation was confirmed by measuring the Mn metal ion concentration using an inductively coupled plasma atomic emission spectroscopy (ICP-AES, Optima 7300 DV ICP-AES, PerkinElmer Ltd, Boston, MA, USA) method.

2.3. Animals

TgCRND8 transgenic mice (AD mice) and their wild type (WT) littermates were bred at the Krembil Discovery Tower (KDT), Toronto, ON, Canada [23], and were transferred for experimental work to the Spatio-Temporal Targeting and Amplification of Radiation Response (STTARR) facility within the University Health Network (UHN). All experiments were approved by the Animal Care Committee at UHN. The TgCRND8+ AD mouse strain was developed and characterized as previously described [23]. Random distributions of male and female mice were used in the experiments to minimize any possible bias, and the observer blinded as to treatment. All animal care procedures undertaken were performed in accordance with the Guide to the Care and Use of Experimental Animals established by the Canadian Council of Animal Care and were approved by the UHN Animal Care Committee (AUP 5703).

2.4. [¹⁸F]FDG-PET/CT imaging

Six-month-old AD mice were treated IV with 100 μ mol Mn/kg b.w. of Ab-TP-MDNPs or vehicle control twice weekly for 2 weeks. The animals were subjected to [¹⁸F]FDG-PET/CT measurement 3 days prior to (baseline) and 3 days after the last treatment (post-treatment measurement). The animals underwent overnight fasting before the scan and blood glucose concentration was obtained from a blood sample prior to radiotracer injection to ensure adequate cerebral absorption of the glucose upon administration of [¹⁸F]FDG radiotracer. Then, the animals received intravenous [¹⁸F]FDG (8.80–20.11 MBq; mean 13.52 MBq) 60 min before the [¹⁸F]FDG-PET scan for 20 min. The [¹⁸F]FDG-PET images were reconstructed using ordered subset expectation maximization (OSEM) with 4 subsets, 4 iterations as well as attenuation and scatter correction. The reconstructed PET resolution was 400 μ m isotropic. Prior to PET imaging, CT images were acquired with 50 kVp, 980 μ A and

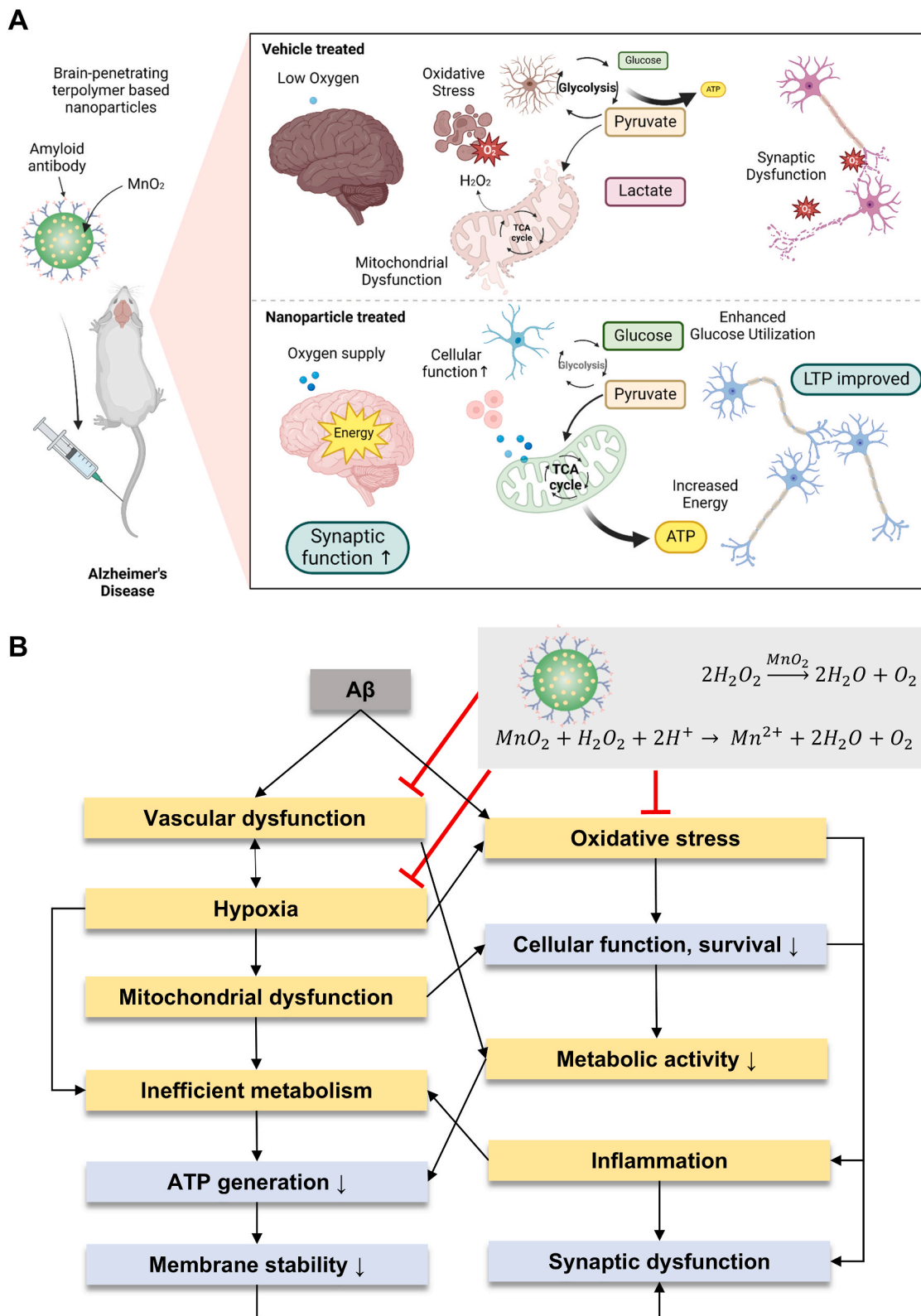


Fig. 1. Schematics illustrating proposed effects of Ab-TP-MDNP treatment in the brain of a mouse model of AD. (A) Intravenously administered Ab-TP-MDNPs can exert several beneficial effects, including generating oxygen, reducing local oxidative stress, enhancing the mitochondrial TCA cycle to promote more efficient energy production in affected neurons. The improved production of local adenosine triphosphate (ATP) in affected brain regions aids in promoting neuronal synaptic signaling, ultimately promoting better cognitive network activity and memory retention. (B) Schematic diagram showing that the basic chemical reaction of manganese dioxide in the Ab-TP-MDNPs. This activity can block Aβ-induced oxidative stress and associated vascular dysfunction resulting in hypoxia which can compromise mitochondrial function, ATP production and triggers ROS generation. These events within the brain microenvironment culminate in altered metabolic activity in the brain.

300 msec exposure time. CT scans were reconstructed using voxel and slice thickness settings resulting in an isotropic voxel size of 125 μm . PET and CT images were automatically co-registered with Mediso's Nucline nanoScan® 3.00.020.0000 software (Budapest, Hungary). Images were analyzed using Brain Atlas software (Invivo VivoQuant® 2021, Boston, MA, US) for automated brain segmentation and derivation of regional PET uptake volumes-of-interest (Siemens, Berlin, Germany).

2.5. Immunohistochemistry

Mouse brains were harvested following perfusion with saline, followed by 10% neutral buffered formalin. Tissues were then processed and embedded in paraffin. Sectioning was performed on a Leica RM2125 microtome (Wetzlar, Germany) at 7 μm . Following heating, sections were processed through a series of xylene and ethanol baths prior to rehydration. Sections were then treated with 3% H_2O_2 for 15 min at room temperature to inactivate endogenous peroxidase activity for 40 min in methanol containing 1% H_2O_2 . Briefly following rehydration endogenous peroxidases were quenched by incubating the sections for 40 min in methanol-containing 1% H_2O_2 . Following rinsing, sections were stained with primary antibodies against MCT2 (sc-166925 HRP, Santa Cruz, Dallas, TX, USA) following the manufacturer's instructions overnight at 4 °C. Following washing in blocking buffer for 3 × 5 min, this was followed by 1 h in goat anti-rabbit IgG, washed, and 1 h in avidin-HRP at room temperature. Sides were visualized by 5–10 min exposure in diaminobenzidine (DAB, 1 mg/ml in 0.1 M Tris-HCl [pH 7.5]) with hydrogen peroxide (0.03 % final concentration). Counterstaining was performed using CAT hematoxylin (CATHE-MM, 1:5, BioCare Medical, Etobicoke, ON, Canada) for 2–5 min for each slide. Slides were covered with either EcoMount (BioCare Medical, Etobicoke, ON, Canada) or Vector Express Mounting Medium (H-5700, Vector Laboratories, Newark, CA, USA) and visualized under a Hamamatsu Nanoscope 2.0HT (Hamamatsu Photonics, Shizuoka, Japan) slide scanning microscope at 20x or 40x magnification. Images were analyzed and quantified using Hamamatsu NDP.view2 and ImageJ software.

2.6. Western blotting assay

Brains were homogenized in 1 mL of 1x radio-immunoprecipitation assay buffer (RIPA) buffer (pH 8.0) supplemented with 100 μL of 1X protease inhibitor mixture, and 200 μL each of 1x phosphatase inhibitor mixtures 1 and 2 (Sigma-Aldrich, St. Louis, MO, USA) per 10 mL of ice-cold buffer. One ml of buffer was used per 40 mg of brain tissue dissociated using a homogenizer (Fisher Scientific High Viscosity Homogenizer PowerGen 1000 S1, Waltham, MA, USA). Following 15 min of dissociation in ice-cold buffer, homogenates were centrifuged at 14,000 × g for 10 min and the supernatants obtained. Protein concentration was determined by Pierce BCA Protein Assay Kit (Thermo Scientific, Waltham, MA, USA). Protein samples were heated at 95 °C in 4X sample loading buffer (final: 2 % SDS) for 5 min prior to addition and separation by polyacrylamide gel electrophoresis (Bio-Rad, Hercules, CA, USA). Samples were then transferred onto polyvinylidene difluoride (PVDF) membranes (Bio-Rad, Hercules, CA, USA) for electrophoretic transfer. Following 1 h of blocking in 5% goat sera 0.1% Tween-20, PVDF membranes were incubated with primary anti-OGlcNAc (1:1000, 9875, Cell Signaling, Danvers, MA, USA), TOMM20 (1:10000, Ab186735, Abcam, Mississauga, ON, Canada), synaptophysin (1:2000, Ab52636, Abcam, Mississauga, ON, Canada), PSD-95 (1:1000, Ab18258, Abcam, Mississauga, ON, Canada), p-AKT (1:2000, #4060, Cell Signaling, Danvers, MA, USA), or anti- β -actin antibody (1:1000, Ab8226, Abcam, Mississauga, ON, Canada) at room temperature for 1 h. The membranes were then washed and incubated with appropriate secondary antibodies for 1 h prior to luminol-based development using enhanced chemiluminescence horseradish peroxidase substrate (Thermo Scientific, Waltham, MA, USA), with images captured by ChemiDoc MP Imaging System (Bio-Rad, Hercules, CA, USA), and

analyzed by Image Lab Software (Bio-Rad, Hercules, CA, USA). The band intensities of the target proteins were normalized to β -actin for each treatment group.

2.7. Enzyme-linked immunosorbent assay (ELISA)

AD mouse brains were removed from mice 24 h after the last treatment of Ab-TP-MDNPs. Whole brains were homogenized as described above. Supernatant were then collected and used to measure protein content of mouse neprilysin (EM55RB, Invitrogen, Waltham, MA, USA) as per the manufacturer's instructions. xMark Microplate Absorbance Spectrophotometer (Bio-Rad Hercules, CA, USA) was used to measure the level of neprilysin.

2.8. ATP bioluminescence assay, enzymatic lactate assay

AD mouse brains were removed 24 h following their final treatment with Ab-TP-MDNPs. Whole brains were homogenized as described above. Supernatants were then collected and monitored for lactate (Ab65530, Abcam, Mississauga, ON, Canada) and ATP levels (11699709001, Roche, Basel, Switzerland) as per the manufacturer's instructions. Xenogen IVIS spectrum imager (Caliper Life Sciences, Hopkinton, MA, USA) was used to measure the ATP level, and xMark Microplate Absorbance Spectrophotometer (Bio-Rad, Hercules, CA, USA) was used to measure the lactate level.

2.9. Live imaging of primary cortical neurons

Eight-well chambered glass coverslips (Nunc, 12565338) were coated with 0.1 mg/ml poly-L-lysine (Sigma, P1399) solution overnight at 4 °C, then washed 3 times with DDI H_2O and allowed to dry for 1 h. Cortices were dissected from post-natal day 0 (PND0) CD-1 mice, the dura removed and gently triturated to dissociated to single cells, filtered through a 70 μm filter, and numbers of trypan blue-excluding (viable) neurons determined following dissociation. 60,000 trypan blue excluding cells were seeded per well of an 8-well plate in 300 μL of DMEM (Sigma, D5796) supplemented with 10 % FBS and 1% penicillin-streptomycin-glutamine (PSG) (Invitrogen, 10378016) for the first 24 h. The following day the media was completely swapped to serum-free Neurobasal media (Gibco, 21103049) supplemented with 2% B-27 (Gibco, 17504044) and 1% PSG. A 50% media swap was performed every 3–4 days. 1 μM cytosine arabinoside (Sigma, C6645) was added after one day in Neurobasal media and refreshed for the first media swap only to inhibit glial cell growth. Neurons were cultured at 37 °C in a humidified 95% air 5% CO_2 for 9–10 days prior to the experiment. On the day of the experiment cells were incubated with 1.5 μM of the live cell nuclear marker Hoechst 33342 (Invitrogen, H1399) for 1 h, after which the media was swapped to fresh Neurobasal media containing 100 nM TMRM (Setareh Biotech, 6275) to monitor mitochondrial activity in real time. Cells were then treated with 5% dextrose vehicle, 15 μM Ab-TP-MDNPs, 50 μM H_2O_2 , or a combination of 15 μM Ab-TP-MDNP/50 μM H_2O_2 and imaged at 37 °C, 5 % CO_2 every 30 min using a WaveFX spinning-disk confocal microscope equipped with a Hamamatsu EM-CCD C9100-13 camera. Images of selected regions were examined using Volocity software starting 1 h after the initiation of treatment and continuing for 6 h following treatment. Images at 6 h were normalized to time zero images. At 6 h, 10 μM calcein AM (Biolegend, 425201) was added to the media and imaged after 30 min to observe overall cell viability.

For testing the effect of Ab-TP-MDNP on oligomeric $\text{A}\beta$ -induced mitochondrial dysfunction, primary neurons were pre-treated with 10 μM oligomeric $\text{A}\beta$ 42 for 9 h, followed by addition of 15 μM Ab-TP-MDNPs for 1 h. Imaging was performed on a Zeiss AxioObserver.Z1 inverted widefield microscope equipped with a Hamamatsu ORCA-Flash 4.0 camera and LCI Chamlide stage-top incubator. Regions were selected Zeiss Zen software (Blue edition).

2.10. Hippocampal slice preparation

Hippocampal slices were prepared as described previously [24,25]. Briefly, six-month old mice were deeply anesthetized with isoflurane (5%) and decapitalized. Brains were rapidly removed and placed in ice-cold ACSF solution 1 containing 205 mM sucrose, 26 mM NaHCO₃, 10 mM glucose, 2.5 mM KCl, 1.25 mM NaH₂PO₄, 5 mM MgSO₄, 0.5 mM CaCl₂. The solution was constantly bubbled with 95% O₂-5% CO₂ and the brain allowed to cool for 2–3 min. The brain was sliced into 350 μm coronal live sections using a vibratome (VT1200 Leica). Slices were then transferred to a holding chamber containing bubbled artificial cerebrospinal fluid (ACSF) solution 2 containing 124 mM NaCl, 26 mM NaHCO₃, 10 mM Glucose, 3 mM KCl, 3 mM NaH₂PO₄, 1 mM MgSO₄, 2 mM CaCl₂. Slices were allowed to recover at 31 °C for 40 min and at room temperature for another 30 min.

2.11. Electrophysiological recordings

Extracellular recording using hippocampal slices were performed in a submerged flow chamber system (Warner Instruments). Oxygenated ACSF was perfused at a rate of 2 ml/min at 31 °C. Bipolar stimulation electrode (FHC: MX21XEP(RM1)) were placed at Schaffer collaterals within the stratum radiatum of hippocampal slices. Recording electrodes was fabricated with a Sutter P1000 puller and filled with ACSF at 1–2 mΩ resistance placed into the CA1 area. Field excitatory post-synaptic potentials (fEPSP) were measured from recording electrode evoked via stimulation of Schaffer collaterals. Field EPSPs were amplified using a Multiclamp 700B amplifier (Molecular Devices, USA) and digitized at 40 kHz. WinLTP software was used to record the fEPSPs onto PC computer. Stimuli (100 μs duration) were delivered once every 30 s using a DS3 constant current stimulation isolator (Digitimer, UK). After obtaining optimal fEPSPs, electrodes were allowed to stabilize for 10 min. Input-output curve was generated by gradually increasing the stimulation intensity. Online real-time data analysis was monitored to ensure a stable baseline, following stable baseline recording for 30 min, a compressed theta burst was given (cTBS, each TBS consisted of 5 burst at 5 Hz, with each burst composed of 5 pulses at 100 Hz, three TBS episodes were delivered at 10 s interval), delivered to induce long term potentiation (LTP). Following cTBS stimulation, a subsequent 1-h recording was performed.

2.12. Electrophysiology data analysis

Data are presented as mean ± SEM. N represents number of slices from different animals. Rising slope of fEPSPs was analyzed to examine response intensity. The amplitude of fiber volleys was analyzed for input output curve. For LTP experiments responses were normalized to the last 5 min of baseline prior to cTBS stimulation. Statistical significance was assessed using one-way ANOVA and followed by post hoc LSD multiple comparison test (SPSS). For input output curve statistics, repeated measures ANOVA was used and followed by post hoc LSD multiple comparison test (SPSS). Significance is denoted as * $p \leq 0.05$.

2.13. Statistical analysis

Statistical analysis was performed using GraphPad Prism 9 (San Diego, CA, USA). Data were analyzed using either *t*-test, Fisher's exact test, or ANOVA test followed by Tukey's multiple comparison test as appropriate. Data are represented as mean ± SD. $p < 0.05$ results were considered statistically significant.

3. Results

3.1. Ab-TP-MDNPs increase cerebral glucose utilization

In light of the pivotal role of oxidative stress and hypoxia in cerebral

glucose metabolism in AD mice, we investigated the therapeutic effects of Ab-TP-MDNPs on cerebral glucose utilization *in vivo* using [¹⁸F]FDG-PET/CT imaging. In conjunction with CT such imaging allows for the localization and segmentation of glucose uptake in different brain compartments (Fig. 2A-1, 2A-2), [¹⁸F]FDG-PET is the most validated imaging modality to measure glucose utilization in the brain using radiotracers [7]. Ab-TP-MDNPs were synthesized as previously described [16] (Fig. S1) and administered intravenously twice a week for two weeks. To access brain function, PET/CT scans were performed before and following treatment (Figs. 2A–3). The pre-treatment scans for each animal served as their respective baseline measurements to account for individual variability. After 2 weeks of treatment an increase in cerebral glucose utilization was observed in several brain regions, including the cortex and hippocampus. Compared to vehicle (Veh) controls, Ab-TP-MDNP treatment resulted in an increase of 35–70% in cerebral glucose utilization, depending on the region, with a remarkable 48% increase in the cortex, and 66% increase in the hippocampus, without altering the expression level of glucose transporter protein type 3 (GLUT3) in the brain (Fig. S2). By contrast cerebral glucose utilization in the control treatment group exhibited a decreasing trend below the baseline, while Ab-TP-MDNP treatment showed an increase of 31–46% above the baseline. Remarkably Ab-TP-MDNP treatment demonstrated an increase in cerebral glucose utilization across all brain regions, implying a widespread and comprehensive impact of nanoparticles on oxidative stress and hypoxia throughout the brain during the brief period of AD treatment in our studies.

3.2. Ab-TP-MDNPs improve glucose metabolic efficiency

The brain microenvironment of AD plaques presents regions of low oxygen, promoting a shift in metabolism toward glycolysis reducing available neuronal ATP [26,27]. Owing to the reactivity of encapsulated MnO₂ along with the disease site-targetability, Ab-TP-MDNPs can locally generate oxygen in regions of AD injury containing elevated concentration of H₂O₂ [16,22], which may induce more efficient oxidative phosphorylation (Fig. 1B).

A consequence of poor glucose utilization linked to AD is the presence of O-linked-N-acetylglucosamylation (OGlcNAc) post-translational modification of proteins, which arise under conditions of abundant glucose [28], known to exhibit protective effects against the AD-induced toxicity [29]. Consistent with increased glucose utilization in AD brain shown in Fig. 2, Ab-TP-MDNPs increased the levels of OGlcNAc by 70% (Fig. 3A).

Owing to high lipid content, regions of significant free radical generation in neurons such as the mitochondria in neurons are strikingly susceptible to the effects of hypoxia and oxidative stress [30]. To exacerbate these effects, the high glucose consumption and energetic demand of neurons make them vulnerable to even brief interruptions in oxygen supply; particularly if vascular availability to glucose is already limited [5]. Because of this, mitochondrial dysfunction is known to contribute significantly to the observed effects of AD [26,31]. To study the influence of anti-oxidant and oxygen-generating Ab-TP-MDNPs on mitochondria in AD mouse brain, we determined the level of translocase of the outer mitochondrial membrane complex subunit TOMM20. As shown in Fig. 3B, levels of TOMM20 in the whole brain homogenates increased 25% following 2 weeks of Ab-TP-MDNPs treatment. Because of efficient delivery of glucose to brain cells and improved mitochondrial function, ATP levels were observed to increase 32% following treatment within the brain microenvironment (Fig. 3C), improving critical energy resources for impaired neurons. A consequence of improved mitochondrial function and enhanced oxygen production from Ab-TP-MDNPs treatment can shift the glucose metabolism into more efficient oxidative phosphorylation from anaerobic glycolysis. To investigate the effects of Ab-TP-MDNPs on metabolic reprogramming, we measured lactate levels in whole brain homogenates following Ab-TP-MDNPs treatment. As shown in Fig. 3D, Ab-TP-MDNPs treatment

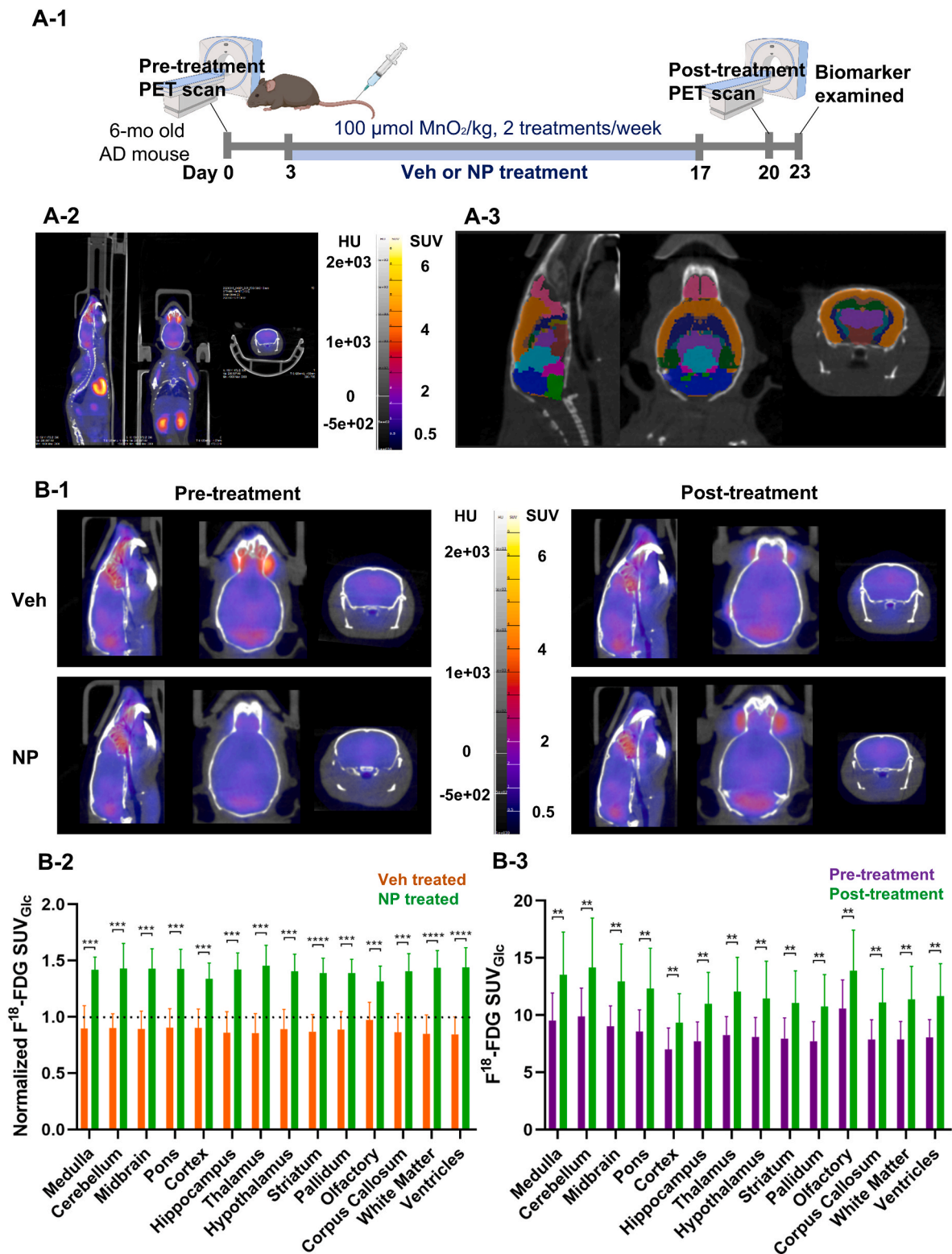
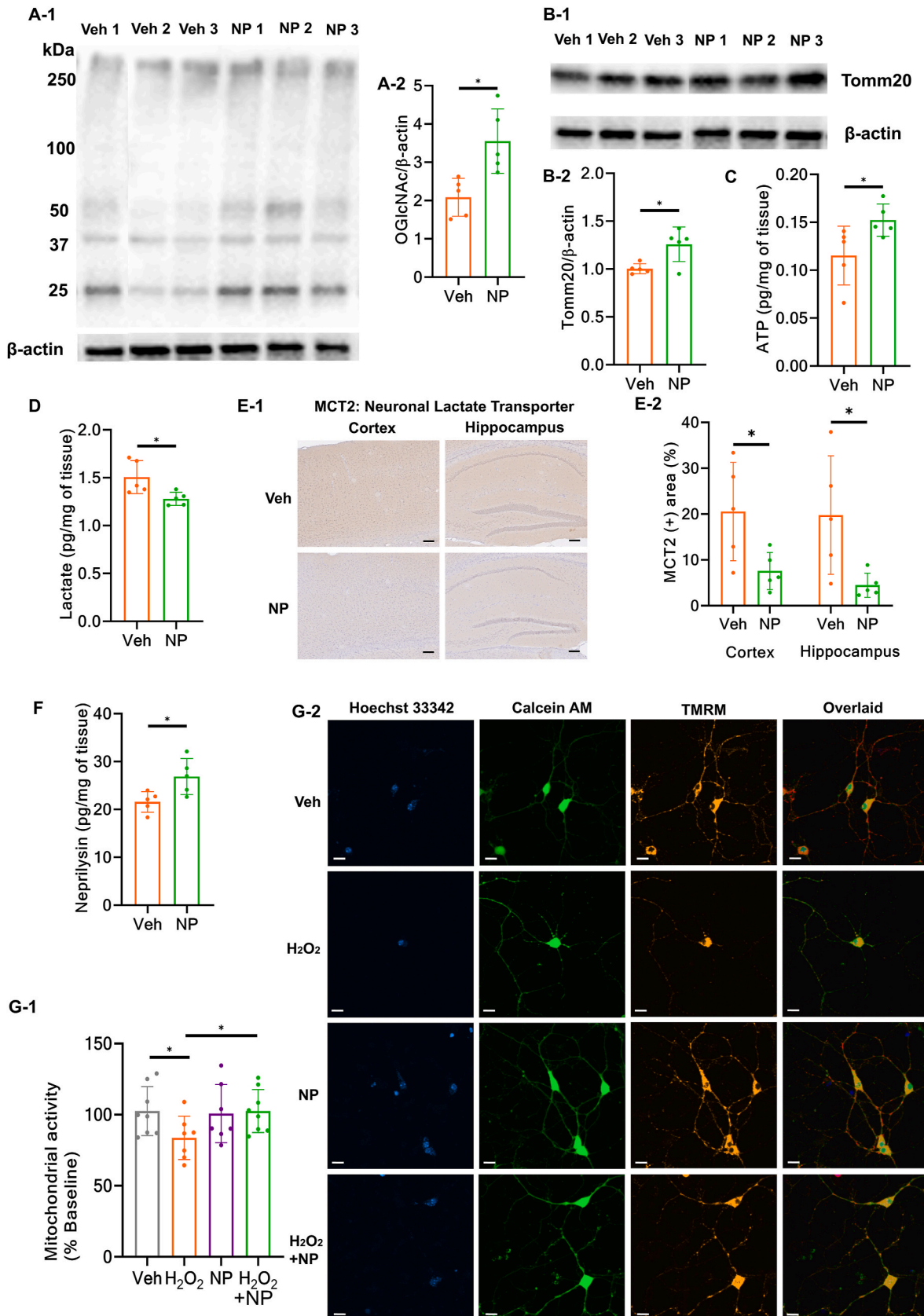


Fig. 2. Ab-TP-MDNPs improve glucose utilization in AD brain. (A-1) Representative example of [^{18}F]FDG-PET/CT scan in the experimental group. (A-2) Example of 6-month old AD mouse (random distributions of male and female mice) treated IV with 100 $\mu\text{mol MnO}_2/\text{kg}$ body weight (b.w.) of Ab-TP-MDNPs (NP) or vehicle (Veh) (4% dextrose) (control group) twice weekly for 2 weeks, [^{18}F]FDG-PET measurements taken before and after the treatment. (A-3) Representative example of brain segmentation of CT scan using Brain Atlas software. (B) Cerebral glucose utilization assessed by [^{18}F]FDG-PET/CT in AD mouse brain pre- and post-treatment with either Ab-TP-MDNPs or Veh, (B-1) representative brain images are shown. (B-2) Cerebral glucose utilization values were normalized by individual pre-treatment values and compared between two treatment groups. (B-3) Cerebral glucose utilization was compared between pre- and post-treatment within the Ab-TP-MDNPs treated animals. Scale bar equals 100 μm . The data are presented as mean \pm SD (n = 6 per group). Individual values are presented as dots for both vehicle and NP-treated mice. Asterisk(s) (*) denotes a significant difference at *p < 0.05, **p < 0.01, ***p < 0.0001) compared to vehicle treatment. N.S. – not significant.



(caption on next page)

Fig. 3. Ab-TP-MDNPs improve the efficiency of glucose metabolism. Six-month old AD mice (random distribution, male and female mice) were treated IV with 100 $\mu\text{mol Mn/kg}$ body weight of Ab-TP-MDNPs (NP) or vehicle (Veh) (4% dextrose) (control group) twice weekly for 2 weeks (Fig. 3A–F, Treatment schedule follows that in Fig. 2A, $n = 5$ per treatment group). (A) Western blot analysis for OGlcnAc in whole brain homogenates of either Ab-TP-MDNPs or Veh treated animals showing 3 representative band images (A-1) and its analysis (A-2). (B) Western blot for TOMM20 (outer mitochondrial marker) in whole brain homogenates of either Ab-TP-MDNPs or Veh treated animals showing 3 representative band images (B-1) and its analysis (B-2). (C) Level of ATP measured by ATP bioluminescence kit in the AD brain homogenates. (D) Level of lactate measured by enzymatic lactate assay kit in the AD brain homogenates. (E) Representative IHC images (E-1) and corresponding quantification (E-2) of the neuronal lactate transporter MCT2, in the hippocampus and cortex of AD mouse brain. The scale bar corresponds to 100 μm . (F) Levels of neprilysin as measured by ELISA in the AD brain homogenates. For Fig. 3A–F, data are presented as mean \pm SD. Individual values are shown (dots) for both vehicle and NP-treated mice. (G) Effect of Ab-TP-MDNPs on mitochondrial activity: Quantification plots (G-1) and representative CLSM images (G-2) demonstrating the effects of Ab-TP-MDNPs on mitochondrial activity in mouse cortical neurons following H_2O_2 treatment. Data are presented as mean \pm SD ($n = 8$). Scale bar represents 20 μm . Asterisk (*) denotes a significant difference at $p < 0.05$ compared to vehicle treatment.

promoted a reduction in brain lactate levels by 15%, consistent with improved mitochondrial function in the treated AD brain (Fig. 3B). Similarly, consistent with a drop in local lactate, Ab-TP-MDNP treatment reduced expression of monocarboxylate transporter 2 (MCT2), the major neuronal lactate transporter in the brain by 63% in the cortex and 77% in the hippocampus (Fig. 3E). In addition, we determined the expression of neprilysin, a major $\text{A}\beta$ degrading enzyme whose regulation is suppressed by hypoxia, and found that the treatment with Ab-TP-MDNPs increased its level by 25%, which could enhance $\text{A}\beta$ clearance from the brain (Fig. 3F).

To further investigate the effects of Ab-TP-MDNPs on mitochondrial function in real time, we examined mouse cortical neurons *in vitro*, monitoring both mitochondrial potential using tetramethylrhodamine (TMRM) together with a marker of overall cell viability (Calcein AM) in the presence of H_2O_2 (Fig. 3G). While treatment with Ab-TP-MDNPs alone did not alter cell viability or mitochondrial activity, introduction of H_2O_2 to primary cortical neurons exhibited an acute and significant reduction of mitochondrial membrane potential in the presence of 50 μM H_2O_2 with retraction of neurites over a period of 24 h (Figs. 3G–2, H_2O_2). By contrast, treatment with Ab-TP-MDNPs in the presence of H_2O_2 noticeably protected neuronal morphology and mitochondrial activity (Figs. 3G–2). Given the known effects of $\text{A}\beta$ oligomers on neuroinflammation and ROS generation, we further examined the ability of Ab-TP-MDNPs against oligomeric $\text{A}\beta$ -induced mitochondrial dysfunction. As shown in Fig. S4, Ab-TP-MDNPs treatment reduced $\text{A}\beta$ -induced damages in mitochondrial activity of the primary neuronal culture.

3.3. Ab-TP-MDNPs enhances synaptic function

Impaired glucose metabolism and lack of ATP can adversely affect neuronal function, including memory formation in the brain. A critical aspect of memory formation involves activity-dependent strengthening of synaptic response following high-frequency stimulation, termed long-term potentiation (LTP) [32]. To study the potential of Ab-TP-MDNPs on enhancing synaptic function, Schaffer collateral stimulation-induced field excitatory postsynaptic potentials (fEPSP) were recorded extracellularly in the CA1 striatum radiatum region of hippocampus from coronal mouse slices. As shown in Fig. 5A, cTBS stimulation induced a reliable LTP (177.52 ± 7.95 compared to baseline) from WT mice. Though the current set did not achieve statistical insignificance due to inherent high variation in these animals, the same cTBS stimulation induced reduced LTP (157.50 ± 12.33) in AD mice compared to WT controls, in line with the previous reports on hippocampal synaptic disruption in TgCRND8 mice [33]. As shown in 4B-3, impaired LTP in AD mice treated with Veh (157.50 ± 12.33) was fully rescued by Ab-TP-MDNPs treatment (202.45 ± 13.29). Basal excitatory synaptic transmission was reduced in both treatment groups in AD mice, as assessed by their input-output (I/O) curve. Consistently, maximal synaptic response was observed to be reduced in AD mice (WT = 1.73 ± 0.16 mV, Veh treated AD = 0.82 ± 0.24 mV, NP treated AD = 0.64 ± 0.09 mV). These results suggest that Ab-TP-MDNP treatment may have therapeutic effects on mitigating LTP dysfunction. Western blotting examining synaptic proteins 2 weeks following Ab-TP-MDNP treatment also supports a role in synaptic function in that Ab-TP-MDNP increased

presynaptic levels of presynaptic protein synaptophysin by 35% (Fig. 4C). Postsynaptic density protein 95 (PSD-95) demonstrated a trend toward increasing expression but was not statistically significant. Consistent with their role in promoting hippocampal LTP and synaptic plasticity [34,35], levels of phosphorylated PKB/Akhenaten (p-AKT) increased by 102% following Ab-TP-MDNP treatment. These results suggest that Ab-TP-MDNPs treatment can improve synaptic function and enhance LTP in this AD mouse model.

3.4. Histopathological evaluation of long-term Ab-TP-MDNP treatment

As an initial step to assess the relative safety of this novel AD treatment, we conducted the histopathology examination of major organs in animals treated with Ab-TP-MDNPs over 8 weeks period. Representative histological images of the major organs are presented in Fig. 5A, along with the independent pathologist report included in the supplemental materials (Fig. S5). Histopathological analysis revealed no significant adverse effects the major organs of Ab-TP-MDNPs treated animals as compared to those in the control group treated with vehicle (Veh). Furthermore, we monitored the body weight of the animal throughout the 8 weeks of treatment and found no significant changes following Ab-TP-MDNP treatment (Fig. S3). These results collectively support the relative safety of Ab-TP-MDNP treatment as a potential disease-modifying therapy for AD.

4. Discussion

Our studies have demonstrated the ability of Ab-TP-MDNPs to reach disease-affected regions in the brain and effectively address cerebral glucose metabolism and synaptic function, which are critical to the development of AD. Following IV administration, Ab-TP-MDNPs were successfully transported to the brain through a terpolymer-based brain-drug delivery platform and improved the efficiency of glucose utilization and induced metabolic reprogramming in part by improved mitochondrial function, leading to enhanced ATP generation. Consequently, this approach was observed to improve synaptic function likely through the provision of additional energy resources to brain to promote proper neuronal function, contributing to the multifunctional actions of Ab-TP-MDNPs that break the pathological and pathogenetic cycles [22].

Ab-TP-MDNPs effectively enhanced glucose utilization in the brains of the moderate stage of AD. Ab-TP-MDNPs treatment appears to exert these effects by reducing oxidative stress and hypoxia, which represent substantial roles in the pathology of AD. Hypoxia and oxidative stress are thought to trigger vascular dysfunction through aberrant activation of angiogenesis in part through the hypoxia-inducible factor-1 (HIF-1)/Vascular endothelial growth factor (VEGF) pathway, inducing disruption in the development and contractility of vessels [36,37]. Impaired blood flow consequently impedes the delivery of essential nutrition and oxygen required for brain metabolism, reducing the energy substrates for normal function [22,38]. Consistent with this, control treated animals exhibited a decreasing trend in cerebral glucose utilization even during the 3 weeks of experiment, indicative of disease progression toward advanced stage. In contrast, Ab-TP-MDNPs treatment effectively counteracted and rescued the hypometabolic state induced by AD in the

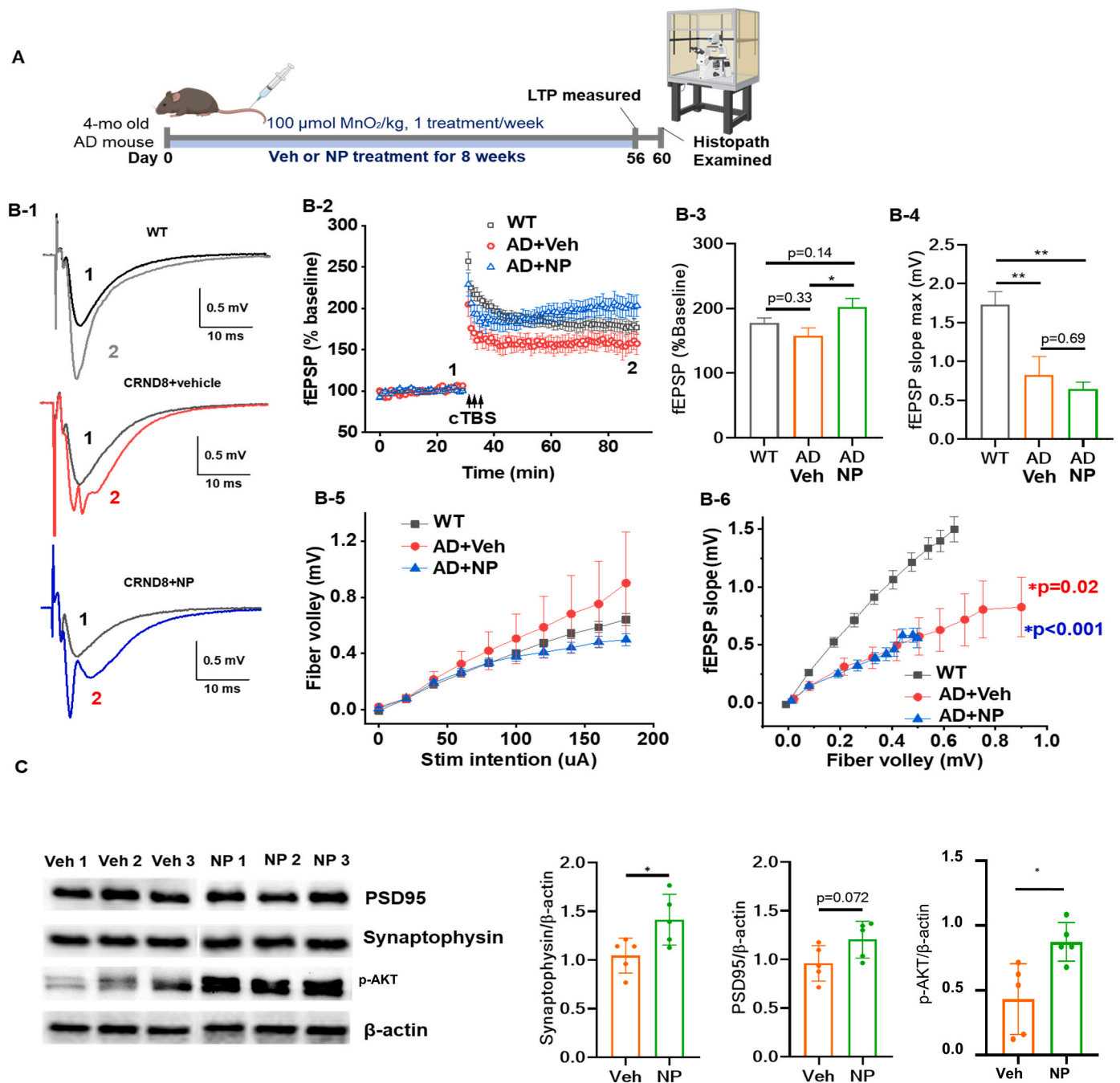


Fig. 4. Ab-TP-MDNPs enhance LTP and synaptic function in an AD mouse model. (A) Four-month (mo) old AD mice (random distribution, male/female) were treated IV with 100 $\mu\text{mol Mn/kg}$ body weight (b.w.) of Ab-TP-MDNPs (NP) or vehicle (Veh, 4% dextrose) weekly for 8 weeks and LTP measured via electrophysiological recording. (B) Field recording of hippocampal slices for untreated WT versus Veh or NP-treated AD mice ($n = 8\text{--}20$ per group). (B-1) Representative traces from immediately before cTBS or 5 min following final cTBS. (B-2) Evoked field EPSPs recorded from the CA1 of mice slices. cTBS stimulation induced a reliable LTP (177.52 ± 7.95 of baseline - grey) in WT controls. cTBS induced reduced LTP (157.50 ± 12.33 , red) in Veh treated AD mice, while LTP was fully restored in Ab-TP-MDNPs treated AD mice (202.45 ± 13.29 , blue). (B-3) Graphical LTP representation of Ab-TP-MDNPs treatment in AD mice. (B-4) Summary bar graph presenting impaired maximal synaptic response of AD animals treated with either Veh or NP and WT mice. (B-5) Input output (I/O) curve relating the stimulation intensity and presynaptic fiber volley amplitude. (B-6) I/O curve relating slope of the fEPSPs to presynaptic fiber volleys at various stimulation intensity. (C) Representative images of Western blot analysis for PSD-95, synaptophysin and quantification of these markers and p-AKT of whole brain homogenates for vehicle or Ab-TP-MDNPs treated animals. Six-month (mo) old AD mice (randomly distributed male and female mice) were treated IV with 100 $\mu\text{mol Mn/kg}$ body weight (b.w.) of Ab-TP-MDNPs (NP) or vehicle (Veh) (4% dextrose) (control group) twice weekly for 2 weeks (Treatment schedule follows that in Fig. 2A). The data are presented as mean \pm SD ($n = 5\text{--}10$ per group). Asterisk(s) (*) denotes a significant difference at $*p < 0.05$ compared to vehicle treatment. N.S. – not significant. (For interpretation of the references to colour in this figure legend, the reader is referred to the Web version of this article.)

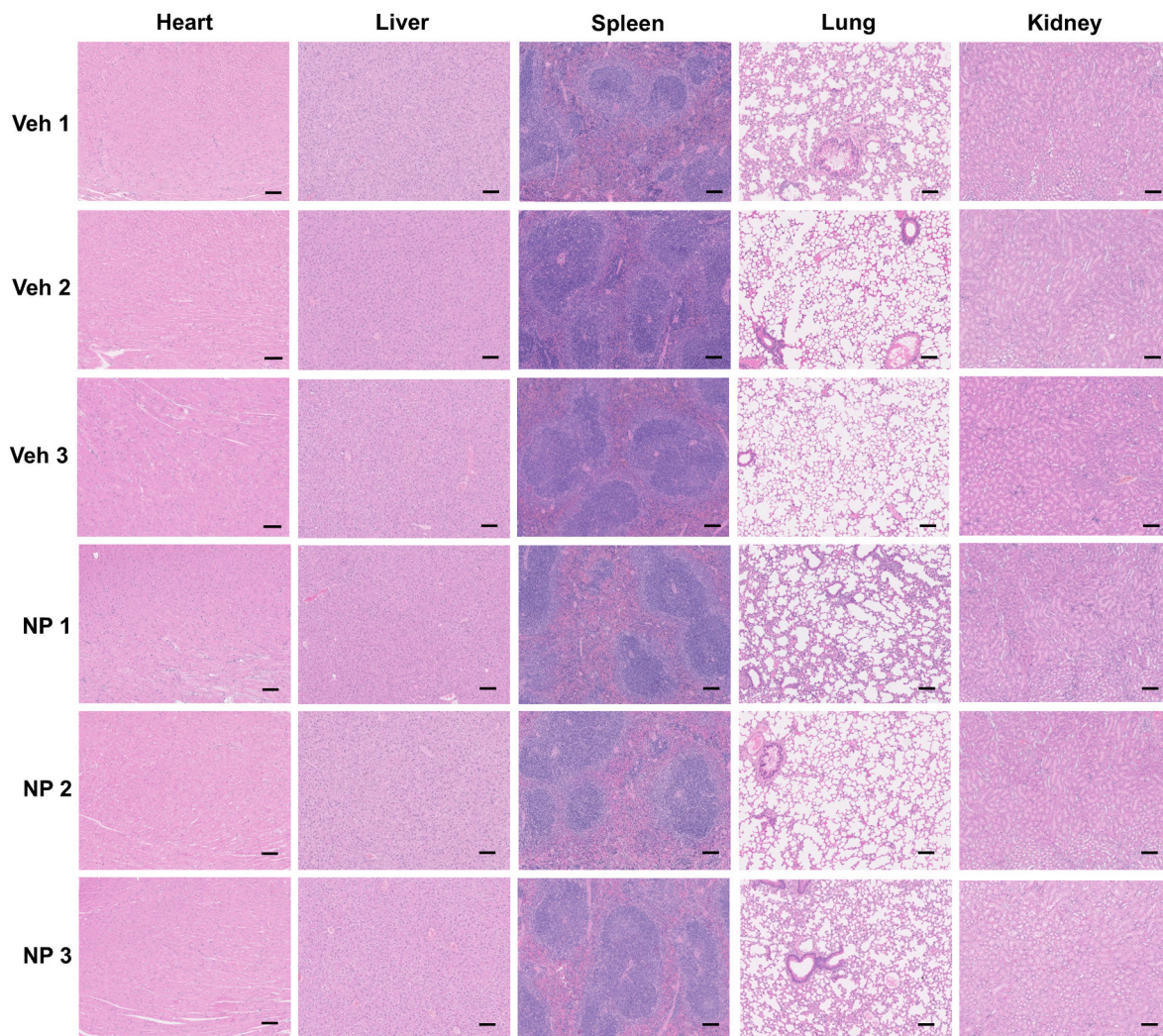


Fig. 5. Repeated i.v. injection of Ab-TP-MDNPs for 8 weeks does not induce pathological morphology. Histopathology analysis of major body organs of AD mice after long-term Ab-TP-MDNPs treatment. Four-month (mo) old AD mice (random distribution of male and female mice) were treated IV with 100 $\mu\text{mol Mn/kg}$ body weight (b.w.) of Ab-TP-MDNPs (NP, green) or vehicle (Veh) (4% dextrose) (control group, orange) once weekly for 8 weeks (Treatment schedule follows that in Fig. 4A). Representative images of H&E-stained major body organs (heart, liver, spleen, lungs, and kidneys) of mice treated with Ab-TP-MDNPs (NP) or vehicle (Veh) (4% dextrose) (control group). Scale bar equals 100 μm . No significant change in the Ab-TP-MDNPs treatment groups was found. (For interpretation of the references to colour in this figure legend, the reader is referred to the Web version of this article.)

brain, which occurred across several regions of the brain.

AD is associated with reduced cerebral glucose utilization across multiple regions of the brain, as supported by both preclinical and clinical data [39,40]. In addition to the medial temporal lobe, AD pathology disrupts neuronal functions in a variety of centers of the brain, particularly as the disease advances [41]. Our findings demonstrate that the therapeutic effects of Ab-TP-MDNPs are not confined to a specific region, but rather may promote these effects over disseminated brain regions wherever pathology exists.

The presence of hypoxia and oxidative stress can induce alterations in the aerobic versus anaerobic mechanisms by which glucose is utilized to create ATP [42]. Such shifts in the glucose metabolism reduces ATP within the localized brain microenvironment (30–38 ATPs vs. 2 ATPs). Impairment in the ability to efficiently utilize glucose is additionally exacerbated by mitochondrial dysfunction arising from neuronal hypoxia and oxidative stress [43], which further impair glucose utilization [44]. Ab-TP-MDNPs treatment aids in re-establishing glucose metabolism by enhancing aerobic environment, resulting in a more abundant cellular ATP supply. Apart from its intracellular functions in neurons, persistent glycolytic activity impairs the microglial ability to detect and remove A β , potentially exacerbated by histone lactylation [45,46].

Interestingly, a decrease in lactate transporters was observed in animals treated with Ab-TP-MDNPs, which may be an adaptive response to the reduction in lactate production upon metabolic reprogramming.

While the involvement of OGlcnAc is well-acknowledged in the pathology of diabetes, recent research has revealed its implication in AD [29]. Like phosphorylation, OGlcnAc controls biochemical signaling by altering the stability or activity of the proteins. Within the brain, the expression of OGlcnAc enzymes have been shown to be 10-fold higher than in peripheral tissues [47], with OGlcnAc playing significant roles in metabolism, stress response, and synaptic plasticity [28]. In the AD, OGlcnAc has been shown to be reduced in response to diminished glucose availability, and this feature has emerged as a potential link between glucose hypometabolism and the progression of AD [48]. Notably, reduced OGlcnAc in amyloid precursor protein or tau can alter its cleavage and phosphorylation, leading to the formation of toxic protein isoforms with their subsequent accumulation in the brain [49]. In our current investigation, Ab-TP-MDNPs treatment exhibited an increase in OGlcnAc level of the proteins in the AD brain, supporting its therapeutic benefits in AD. This could be attributed to the enhanced glucose utilization and availability in the brain from the Ab-TP-MDNPs treatment.

Neurons require higher amounts of energy compared to other cells, utilizing significant portions of their energy toward synaptic transmission and maintenance of resting/action potential [50]. Therefore, lack of sufficient energy reserves in the brain can contribute to synaptic dysfunction, including cellular mechanisms underlying learning and memory [51]. While overtly neuronal survival is not significantly reduced till more advanced stages of AD, synaptic activity is significantly disrupted even before cognitive symptoms are detectable, making it as a most relevant marker for cognitive dysfunction and progression of AD [14,52]. Our findings indicate that Ab-TP-MDNPs treatment can potentially mitigate LTP impairment in AD. Western blotting analysis also showed higher levels of synaptic proteins following Ab-TP-MDNPs treatment, suggesting improved synaptic signaling between neurons, although this treatment did not appear to restore the decreased maximal response of fEPSP. Given the complex synaptic regulation in the brain, further investigations such as the involvement of NMDA receptors, would provide more comprehensive mechanistic insights of the treatment's effects. The capacity of Ab-TP-MDNPs to enhance ATP availability in the brain may facilitate the maintenance of membrane potential and the synthesis and release of neurotransmitters [6]. The correlation between improved synaptic function and elevated glucose utilization could be a chicken-and-egg situation, wherein it is possible that enhanced neuronal activity in response to the treatment leads to an increase in glucose utilization within the brain, or vice versa. Regardless of the precise relationship, these findings demonstrate that Ab-TP-MDNPs treatment improves cerebral glucose utilization and attenuates synaptic dysfunction, which play critical roles in the development and progression of AD.

The findings presented herein offer compelling evidence supporting the therapeutic efficacy of Ab-TP-MDNPs in addressing cerebral glucose metabolism and synaptic function in AD, as evidenced by extensive *in vivo* functional examination using [¹⁸F]FDG-PET/ CT and electrophysiologic examination. Through metabolic reprogramming of glucose utilization, Ab-TP-MDNPs increased the ATP availability thereby supporting proper synaptic function. Our study highlights the promising strategy of combining use of brain-targeting nanotechnology with multi-targeted approaches to achieve enhanced therapeutic effects. By applying this understanding of AD and its affiliated pathways, this strategy advances the field to explore deeper into the development of these disease-modifying treatments not only for AD but other complex neurodegenerative diseases.

CRediT authorship contribution statement

Elliya Park: Writing – original draft, Visualization, Methodology, Investigation, Formal analysis. **Chunsheng He:** Writing – review & editing, Supervision, Project administration, Methodology, Conceptualization. **Azhar Z. Abbasi:** Writing – review & editing, Supervision, Project administration, Methodology. **Meng Tian:** Methodology, Investigation. **Shudi Huang:** Methodology, Investigation. **Liting Wang:** Writing – review & editing, Visualization, Investigation, Formal analysis. **John Georgiou:** Validation, Formal analysis. **Graham L. Colingridge:** Validation. **Paul E. Fraser:** Writing – review & editing, Resources, Funding acquisition. **Jeffrey T. Henderson:** Writing – review & editing, Project administration, Funding acquisition. **Xiao Yu Wu:** Writing – review & editing, Supervision, Funding acquisition, Conceptualization.

Declaration of competing interest

The authors declare that they have no known competing financial interests or personal relationships that could have appeared to influence the work reported in this paper.

Acknowledgements

This work is supported by a Weston Brain Institute Transformational Grant (TR170044) to X.Y.W., J.T.H., P.E.F., Natural Sciences and Engineering Research Council of Canada Equipment Grants (EQPEQ 440689-13) to X.Y.W., Canada Council for the Arts Killam Research Fellowship (7025-18-0051) to X.Y.W, Ontario Graduate Scholarship and departmental top up scholarship to E.P. The synaptic plasticity work was supported by a Krembil Foundation Grant to G.L.C. and J.G. G.L.C. is the holder of the Krembil Family Chair in Alzheimer's Research. The authors also thank A. Elia at University Health Network for the histology services, K. Han at University of Toronto for breeding the TgCRND8+ mouse model, the Spatio-Temporal Targeting and Amplification of Radiation Response (STTARR) program and its affiliated funding agencies for providing the imaging facilities, and the Krembil Research Institute for providing the facilities for the animal work.

Appendix A. Supplementary data

Supplementary data to this article can be found online at <https://doi.org/10.1016/j.biomaterials.2025.123142>.

Data availability

Data will be made available on request.

References

- [1] P. Scheltens, B. De Strooper, M. Kivipelto, H. Holstege, G. Chételat, C.E. Teunissen, J. Cummings, W.M. van der Flier, Alzheimer's disease, *Lancet Lond. Engl.* 397 (2021) 1577–1590, [https://doi.org/10.1016/S0140-6736\(20\)32205-4](https://doi.org/10.1016/S0140-6736(20)32205-4).
- [2] A.I. Levey, Progress with treatments for Alzheimer's disease, *N. Engl. J. Med.* 384 (2021) 1762–1763, <https://doi.org/10.1056/NEJMe2103722>.
- [3] C.E. Conti Filho, L.B. Loss, C. Marcolongo-Pereira, J.V. Rossoni Junior, R. M. Barcelos, O. Chiarelli-Neto, B.S. da Silva, R. Passamani Ambrosio, F.C. de A. Q. Castro, S.F. Teixeira, N.J. Mezzomo, *Advances in Alzheimer's disease's pharmacological treatment*, *Front. Pharmacol.* 14 (2023), <https://doi.org/10.3389/fphar.2023.1101452>.
- [4] C. Ferrari, S. Sorbi, The complexity of Alzheimer's disease: an evolving puzzle, *Physiol. Rev.* 101 (2021) 1047–1081, <https://doi.org/10.1152/physrev.00015.2020>.
- [5] S.M. de la Monte, M. Tong, Brain metabolic dysfunction at the core of Alzheimer's disease, *Biochem. Pharmacol.* 88 (2014) 548–559, <https://doi.org/10.1016/j.bcp.2013.12.012>.
- [6] M.K. Poddar, S. Banerjee, A. Chakraborty, D. Dutta, Metabolic disorder in Alzheimer's disease, *Metab. Brain Dis.* 36 (2021) 781–813, <https://doi.org/10.1007/s11011-021-00673-z>.
- [7] L. Mosconi, Brain glucose metabolism in the early and specific diagnosis of Alzheimer's disease, *Eur. J. Nucl. Med. Mol. Imaging* 32 (2005) 486–510, <https://doi.org/10.1007/s00259-005-1762-7>.
- [8] Y. Dong, G.J. Brewer, Global metabolic shifts in age and Alzheimer's disease mouse brains pivot at NAD⁺/NADH redox sites, *J. Alzheimers Dis.* 71 (2019) 119–140, <https://doi.org/10.3233/JAD-190408>.
- [9] C. Haense, K. Buerger, E. Kalbe, A. Drzezga, S.J. Teipel, P. Markiewicz, K. Herholz, W.D. Heiss, H. Hampel, CSF total and phosphorylated tau protein, regional glucose metabolism and dementia severity in Alzheimer's disease, *Eur. J. Neurol.* 15 (2008) 1155–1162, <https://doi.org/10.1111/j.1468-1331.2008.02274.x>.
- [10] N.J. Jensen, H.Z. Wodschow, M. Nilsson, J. Rungby, Effects of ketone bodies on brain metabolism and function in neurodegenerative diseases, *Int. J. Mol. Sci.* 21 (2020) 8767, <https://doi.org/10.3390/ijms21228767>.
- [11] M. Cai, H. Wang, H. Song, R. Yang, L. Wang, X. Xue, W. Sun, J. Hu, Lactate is answerable for brain function and treating brain diseases: energy substrates and signal molecule, *Front. Nutr.* 9 (2022), <https://doi.org/10.3389/fnut.2022.800901>.
- [12] C.M. Studzinski, W.A. MacKay, T.L. Beckett, S.T. Henderson, M.P. Murphy, P. G. Sullivan, W.M. Burnham, Induction of ketosis may improve mitochondrial function and decrease steady-state amyloid- β precursor protein (APP) levels in the aged dog, *Brain Res.* 1226 (2008) 209–217, <https://doi.org/10.1016/j.brainres.2008.06.005>.
- [13] M.K. Taylor, D.K. Sullivan, J.D. Mahnken, J.M. Burns, R.H. Swerdlow, Feasibility and efficacy data from a ketogenic diet intervention in Alzheimer's disease, *Alzheimers Dement, Transl. Res. Clin. Interv.* 4 (2018) 28–36, <https://doi.org/10.1016/j.trci.2017.11.002>.
- [14] S. Pelucchi, F. Gardoni, M. Di Luca, E. Marcello, Chapter 28 - synaptic dysfunction in early phases of Alzheimer's Disease, in: A. Quartarone, M.F. Ghilardi, F. Boller (Eds.), *Handb. Clin. Neurol.*, Elsevier, 2022, pp. 417–438, <https://doi.org/10.1016/B978-0-12-819410-2.00022-9>.

- [15] Y. Chen, A.K.Y. Fu, N.Y. Ip, Synaptic dysfunction in Alzheimer's disease: mechanisms and therapeutic strategies, *Pharmacol. Ther.* 195 (2019) 186–198, <https://doi.org/10.1016/j.pharmthera.2018.11.006>.
- [16] C. He, T. Ahmed, A.Z. Abbasi, L.Y. Li, W.D. Foltz, P. Cai, E. Knock, P.E. Fraser, A. M. Rauth, J.T. Henderson, X.Y. Wu, Multifunctional bioactive-nanoconstructs for sensitive and accurate MRI of cerebrospinal fluid pathology and intervention of Alzheimer's disease, *Nano Today* 35 (2020) 100965, <https://doi.org/10.1016/j.nantod.2020.100965>.
- [17] J. Li, P. Cai, A. Shalviri, J.T. Henderson, C. He, W.D. Foltz, P. Prasad, P. M. Brodersen, Y. Chen, R. DaCosta, A.M. Rauth, X.Y. Wu, A multifunctional polymeric nanotheranostic system delivers doxorubicin and imaging agents across the blood–brain barrier targeting brain metastases of breast cancer, *ACS Nano* 8 (2014) 9925–9940, <https://doi.org/10.1021/nn501069c>.
- [18] C. He, P. Cai, J. Li, T. Zhang, L. Lin, A.Z. Abbasi, J.T. Henderson, A.M. Rauth, X. Y. Wu, Blood-brain barrier-penetrating amphiphilic polymer nanoparticles deliver docetaxel for the treatment of brain metastases of triple negative breast cancer, *J. Controlled Release* 246 (2017) 98–109, <https://doi.org/10.1016/j.jconrel.2016.12.019>.
- [19] T. Zhang, H. Lip, C. He, P. Cai, J.T. Henderson, A.M. Rauth, X.Y. Wu, Multitargeted nanoparticles deliver synergistic drugs across the blood–brain barrier to brain metastases of triple negative breast cancer cells and tumor-associated macrophages, *Adv. Healthc. Mater.* 8 (2019) 1900543, <https://doi.org/10.1002/adhm.201900543>.
- [20] C. He, J. Li, P. Cai, T. Ahmed, J.T. Henderson, W.D. Foltz, R. Bendayan, A. M. Rauth, X.Y. Wu, Two-step targeted hybrid nanoconstructs increase brain penetration and efficacy of the therapeutic antibody trastuzumab against brain metastasis of HER2-positive breast cancer, *Adv. Funct. Mater.* 28 (2018) 1705668, <https://doi.org/10.1002/adfm.201705668>.
- [21] H.L. Wong, X.Y. Wu, R. Bendayan, Nanotechnological advances for the delivery of CNS therapeutics, *Adv. Drug Deliv. Rev.* 64 (2012) 686–700, <https://doi.org/10.1016/j.addr.2011.10.007>.
- [22] E. Park, L.Y. Li, C. He, A.Z. Abbasi, T. Ahmed, W.D. Foltz, R. O'Flaherty, M. Zain, R. P. Bonin, A.M. Rauth, P.E. Fraser, J.T. Henderson, X.Y. Wu, Brain-penetrating and disease site-targeting manganese dioxide-polymer-lipid hybrid nanoparticles remodel microenvironment of Alzheimer's disease by regulating multiple pathological pathways, *Adv. Sci.* 10 (2023) 2207238, <https://doi.org/10.1002/advs.202207238>.
- [23] M.A. Chishti, D.-S. Yang, C. Janus, A.L. Phinney, P. Horne, J. Pearson, R. Strome, N. Zuker, J. Loukides, J. French, S. Turner, G. Lozza, M. Grilli, S. Kunicki, C. Morissette, J. Paquette, F. Gervais, C. Bergeron, P.E. Fraser, G.A. Carlson, P. S. George-Hyslop, D. Westaway, Early-onset amyloid deposition and cognitive deficits in transgenic mice expressing a double mutant form of amyloid precursor protein 695, *J. Biol. Chem.* 276 (2001) 21562–21570, <https://doi.org/10.1074/jbc.M100710200>.
- [24] P. Park, T.M. Sanderson, M. Amici, S.-L. Choi, Z.A. Bortolotto, M. Zhuo, B.-K. Kaang, G.L. Collingridge, Calcium-permeable AMPA receptors mediate the induction of the protein kinase A-dependent component of long-term potentiation in the Hippocampus, *J. Neurosci.* 36 (2016) 622–631, <https://doi.org/10.1523/JNEUROSCI.3625-15.2016>.
- [25] T.E. Bartlett, J. Lu, Y.T. Wang, Slice orientation and muscarinic acetylcholine receptor activation determine the involvement of N-methyl D-aspartate receptor subunit GluN2B in hippocampal area CA1 long-term depression, *Mol. Brain* 4 (2011) 41, <https://doi.org/10.1186/1756-6606-4-41>.
- [26] G. Yellen, Fueling thought: management of glycolysis and oxidative phosphorylation in neuronal metabolism, *J. Cell Biol.* 217 (2018) 2235–2246, <https://doi.org/10.1083/jcb.201803152>.
- [27] I. Asllani, C. Habeck, N. Scarmeas, A. Borogovac, T.R. Brown, Y. Stern, Multivariate and univariate analysis of continuous arterial spin labeling perfusion MRI in Alzheimer's disease, *J. Cereb. Blood Flow Metab.* 28 (2008) 725–736, <https://doi.org/10.1038/sj.jcbfm.9600570>.
- [28] J. Park, M.K.P. Lai, T.V. Arumugam, D.-G. Jo, O-GlcNAcylation as a therapeutic target for Alzheimer's disease, *NeuroMolecular Med.* 22 (2020) 171–193, <https://doi.org/10.1007/s12017-019-08584-0>.
- [29] Y. Zhu, X. Shan, S.A. Yuzwa, D.J. Vocadlo, The emerging link between O-GlcNAc and Alzheimer disease, *J. Biol. Chem.* 289 (2014) 34472–34481, <https://doi.org/10.1074/jbc.R114.601351>.
- [30] X. Wang, W. Wang, L. Li, G. Perry, H. Lee, X. Zhu, Oxidative stress and mitochondrial dysfunction in Alzheimer's disease, *Biochim. Biophys. Acta BBA - Mol. Basis Dis.* 1842 (2014) 1240–1247, <https://doi.org/10.1016/j.bbadis.2013.10.015>.
- [31] A. Bobba, G. Amadoro, D. Valenti, V. Corsetti, R. Lassandro, A. Atlante, Mitochondrial respiratory chain Complexes I and IV are impaired by β -amyloid via direct interaction and through Complex I-dependent ROS production, respectively, *Mitochondrion* 13 (2013) 298–311, <https://doi.org/10.1016/j.mito.2013.03.008>.
- [32] T.V.P. Bliss, G.L. Collingridge, A synaptic model of memory: long-term potentiation in the hippocampus, *Nature* 361 (1993) 31–39, <https://doi.org/10.1038/361031a0>.
- [33] R. Kimura, D. MacTavish, J. Yang, D. Westaway, J.H. Jhamandas, Beta amyloid-induced depression of hippocampal long-term potentiation is mediated through the amylin receptor, *J. Neurosci.* 32 (2012) 17401–17406, <https://doi.org/10.1523/JNEUROSCI.3028-12.2012>.
- [34] J. Levenska, H. Wong, R.A. Milstead, B.N. Keller, L.E. LaPlante, C.A. Hoeffler, AKT isoforms have distinct hippocampal expression and roles in synaptic plasticity, *Elife* 6 (2017) e30640, <https://doi.org/10.7554/eLife.30640>.
- [35] B.D. Manning, A. Toker, AKT/PKB signaling: navigating the network, *Cell* 169 (2017) 381–405, <https://doi.org/10.1016/j.cell.2017.04.001>.
- [36] R. Nortley, N. Korte, P. Izquierdo, C. Hirunpattarasilp, A. Mishra, Z. Jaunmuktane, V. Kyrygyri, T. Pfeiffer, L. Khennouf, C. Madry, H. Gong, A. Richard-Loendt, W. Huang, T. Saito, T.C. Saido, S. Brandner, H. Sethi, D. Attwell, Amyloid β oligomers constrict human capillaries in Alzheimer's disease via signaling to pericytes, *Science* 365 (2019) eaav9518, <https://doi.org/10.1126/science.aav9518>.
- [37] B.H. Han, M. Zhou, A.W. Johnson, I. Singh, F. Liao, A.K. Vellimana, J.W. Nelson, E. Milner, J.R. Cirrito, J. Basak, M. Yoo, H.H. Dietrich, D.M. Holtzman, G.J. Zipfel, Contribution of reactive oxygen species to cerebral amyloid angiopathy, vasomotor dysfunction, and microhemorrhage in aged Tg2576 mice, *Proc. Natl. Acad. Sci.* 112 (2015) E881–E890, <https://doi.org/10.1073/pnas.1414930112>.
- [38] C.F. Lourenço, A. Ledo, R.M. Barbosa, J. Laranjinha, Neurovascular-neuroenergetic coupling axis in the brain: master regulation by nitric oxide and consequences in aging and neurodegeneration, *Free Radic. Biol. Med.* 108 (2017) 668–682, <https://doi.org/10.1016/j.freeradbiomed.2017.04.026>.
- [39] G. Chételat, J. Arbizu, H. Barthel, V. Garibotto, I. Law, S. Morbelli, E. van de Giessen, F. Agosta, F. Barkhof, D.J. Brooks, M.C. Carrillo, B. Dubois, A.M. Fjell, G. B. Frisoni, O. Hansson, K. Herholz, B.F. Hutton, C.R. Jack, A.A. Lammertsma, S. M. Landau, S. Minoshima, F. Nobili, A. Nordberg, R. Ossenkoppele, W.J.G. Oyen, D. Perani, G.D. Rabinovici, P. Scheltens, V.L. Villemagne, H. Zetterberg, A. Drzezga, Amyloid-PET and 18F-FDG-PET in the diagnostic investigation of Alzheimer's disease and other dementias, *Lancet Neurol.* 19 (2020) 951–962, [https://doi.org/10.1016/S1474-4422\(20\)30314-8](https://doi.org/10.1016/S1474-4422(20)30314-8).
- [40] C. Bouter, C. Irwin, T.N. Franke, N. Beindorff, Y. Bouter, Quantitative brain positron emission tomography in female 5XFAD Alzheimer mice: pathological features and sex-specific alterations, *Front. Med.* 8 (2021), <https://doi.org/10.3389/fmed.2021.745064>.
- [41] H. Hampel, J. Hardy, K. Blennow, C. Chen, G. Perry, S.H. Kim, V.L. Villemagne, P. Aisen, M. Vendruscolo, T. Iwatsubo, C.L. Masters, M. Cho, L. Lannfelt, J. L. Cummings, A. Vergallo, The amyloid- β pathway in Alzheimer's disease, *Mol. Psychiatry* 26 (2021) 5481–5503, <https://doi.org/10.1038/s41380-021-01249-0>.
- [42] S.H. Baik, S. Kang, W. Lee, H. Choi, S. Chung, J.-I. Kim, I. Mook-Jung, A breakdown in metabolic reprogramming causes microglia dysfunction in Alzheimer's disease, *Cell Metab.* 30 (2019) 493–507.e6, <https://doi.org/10.1016/j.cmet.2019.06.005>.
- [43] T. Terada, T. Obi, T. Bunai, T. Matsudaira, E. Yoshikawa, I. Ando, M. Futatsubashi, H. Tsukada, Y. Ouchi, In vivo mitochondrial and glycolytic impairments in patients with Alzheimer disease, *Neurology* 94 (2020) e1592–e1604, <https://doi.org/10.1212/WNL.0000000000009249>.
- [44] S. Bhatt, L. Puli, C.R. Patil, Role of reactive oxygen species in the progression of Alzheimer's disease, *Drug Discov. Today* 26 (2021) 794–803, <https://doi.org/10.1016/j.drudis.2020.12.004>.
- [45] R.-Y. Pan, L. He, J. Zhang, X. Liu, Y. Liao, J. Gao, Y. Liao, Y. Yan, Q. Li, X. Zhou, J. Cheng, Q. Xing, F. Guan, J. Zhang, L. Sun, Z. Yuan, Positive feedback regulation of microglial glucose metabolism by histone H4 lysine 12 lactylation in Alzheimer's disease, *Cell Metab.* 34 (2022) 634–648.e6, <https://doi.org/10.1016/j.cmet.2022.02.013>.
- [46] R. Holland, A.L. McIntosh, O.M. Finucane, V. Mela, A. Rubio-Araiz, G. Timmons, S. A. McCarthy, Y.K. Gun'ko, M.A. Lynch, Inflammatory microglia are glycolytic and iron retentive and typify the microglia in APP/PS1 mice, *Brain Behav. Immun.* 68 (2018) 183–196, <https://doi.org/10.1016/j.bbi.2017.10.017>.
- [47] R. Okuyama, S. Marshall, UDP-N-acetylglucosaminyl transferase (OGT) in brain tissue: temperature sensitivity and subcellular distribution of cytosolic and nuclear enzyme, *J. Neurochem.* 86 (2003) 1271–1280, <https://doi.org/10.1046/j.1471-4159.2003.01939.x>.
- [48] F. Liu, J. Shi, H. Tanimukai, J. Gu, J. Gu, I. Grundke-Iqbal, K. Iqbal, C.-X. Gong, Reduced O-GlcNAcylation links lower brain glucose metabolism and tau pathology in Alzheimer's disease, *Brain* 132 (2009) 1820–1832, <https://doi.org/10.1093/brain/awp099>.
- [49] S. Schedin-Weiss, B. Winblad, L.O. Tjernberg, The role of protein glycosylation in Alzheimer disease, *FEBS J.* 281 (2014) 46–62, <https://doi.org/10.1111/febs.12590>.
- [50] C. Howarth, P. Gleeson, D. Attwell, Updated energy budgets for neural computation in the neocortex and cerebellum, *J. Cereb. Blood Flow Metab.* 32 (2012) 1222–1232, <https://doi.org/10.1038/jcbfm.2012.35>.
- [51] A. Citri, R.C. Malenka, Synaptic plasticity: multiple forms, functions, and mechanisms, *Neuropsychopharmacology* 33 (2008) 18–41, <https://doi.org/10.1038/sj.npp.1301559>.
- [52] S.W. Scheff, D.A. Price, Synaptic pathology in Alzheimer's disease: a review of ultrastructural studies, *Neurobiol. Aging* 24 (2003) 1029–1046, <https://doi.org/10.1016/j.neurobiolaging.2003.08.002>.